ACS APPLIED MATERIALS & INTERFACES

Research Article

www.acsami.org

A New Class of Red Fluorescent Organic Nanoparticles: Noncovalent Fabrication and Cell Imaging Applications

Xiqi Zhang,*,# Xiaoyong Zhang,# Bin Yang, Yaling Zhang, and Yen Wei*

Department of Chemistry and Key Laboratory of Bioorganic Phosphorus Chemistry & Chemical Biology (Ministry of Education), Tsinghua University, Beijing, 100084, P. R. China

Supporting Information

ABSTRACT: Cyano-substituted diarylethlene derivatives **R-OMe** (**-H, -CF_3**) with different peripheral substituted groups were synthesized in high yield. Water-soluble red fluorescent organic nanoparticles (FONs) could be facilely prepared from them via hydrophobic interaction with polyoxyethylene−polyoxypropylene−polyoxyethylene triblock copolymer (Pluronic F127). The optical properties and surface morphology of the synthesized FONs were characterized, and their biocompatibilities as well as their applications in cell imaging were further investigated. We demonstrate that such red FONs exhibit antiaggregation-caused quenching properties, broad excitation wavelengths, excellent water dispersibilities, and biocompatibilities, making them promising for cell imaging.

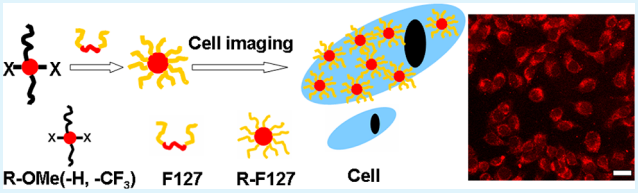

KEYWORDS: *cyano-substituted diarylethlene derivatives, red fluorescent organic nanoparticles, antiaggregation-caused quenching, broad excitation wavelength, cell imaging*

1. INTRODUCTION

The development of optical probes for bioimaging and biomedical applications has attracted considerable research interest over the past few decades.[1] Red/near-infrared (R/NIR, > 600 nm) emission of optical cellular probes is highly desirable for biological applications thanks to their particular advantages of low optical absorption and autofluorescence in biological media.[2,3] So far, a diversity of fluorescent materials, including fluorescent inorganic nanoparticles (FINs),[4,5] fluorescent proteins,[6] and organic dyes,[7] has been used as R/NIR bioprobes. However, most of them often suffer from notorious disadvantages, which severely limits their practical biomedical applications. For example, the usage of fluorescent proteins is often restricted because of the high cost, low molar absorptivity, and low photobleaching thresholds.[8] The vast majority of organic dyes are intrinsicly hydrophobic and unstable in biological media.[9] Quantum dots and FINs are often toxic to living organisms due to their heavy metal toxicity and nonbiodegradable feature.[10] Compared with the currently used optical bioprobes, fluorescent organic nanoparticles (FONs) have recently received increasing attention owing to their biodegradation potential and flexible synthetic approaches of these small organic molecules.[11−13] Various FONs including polydopamine nanoparticles, fluorescent conjugated polymers,[14−21] self-assembled fluorescent nanoparticles,[22−25] and aggregation-induced-emission (AIE) or aggregation induced emission enhancement (AIEE) materials have been successfully prepared in recent years.[26−34] It is worth noting that AIE or AIEE based FONs have extraordinary antiaggregation-caused quenching (anti-ACQ) effect compared to the traditional organic dyes. A wide variety of AIE or AIEE units such as siloles,[35] cyano-substituted diarylethylene,[36,37] tetraphenylethene,[38−41] triphenylethene,[42,43] and distyrylanthracene derivatives[44−47] conjugated molecules has been utilized for chemosensors and bioimaging applications.

In the previous report, we have demonstrated that mixing AIE dyes with a commercial surfactant (Pluronic F127) could facilely encapsulate the hydrophobic AIE dye to form hydrophilic FONs.[48] The obtained FONs are promising for cell imaging and have excellent biocompatibility. However, the maximum emission wavelength of these FONs is less than 540 nm, which is not long enough to avoid interference of the body optical absorption, light scattering, and autofluorescence of biological media, thus limiting their practical bioimaging applications. Therefore, preparation of R/NIR FONs in a facile way is still highly demanded.

In this work, three cyano-substituted diarylethlene derivatives **R-OMe** (**-H, -CF_3**) with different peripheral substituted groups were synthesized in high yield and then facilely prepared as red FONs via hydrophobic−hydrophilic interactions with Pluronic F127 (Scheme 1). The surface morphologies, water solubilities, and optical properties of these FONs were characterized, which showed good water dispersibilities and anti-ACQ properties. The biocompatibilities and cell uptake behavior of such red FONs were further examined to investigate the potential biomedical applications.

Received: December 17, 2013
Accepted: February 20, 2014
Published: February 20, 2014

   dx.doi.org/10.1021/am4058309 | *ACS Appl. Mater. Interfaces* 2014, 6, 3600−3606

Scheme 1. Schematic Illustration of the R-OMe (-H, -CF_3) FONs Preparation Procedure and Their Utilization for Cell Imaging

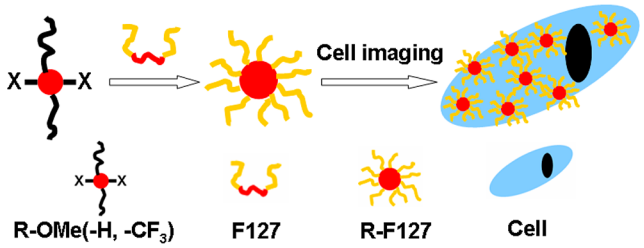

2. EXPERIMENTAL SECTION

2.1. Materials and Measurements. Thiophene, 3-(bromomethyl)heptane, thiophene-2-carboxylic acid, thionyl chloride, dimethylamine, *n*-butyllithium, stannic chloride, 2-(4-methoxyphenyl)-acetonitrile, 2-phenylacetonitrile, 2-(4-(trifluoromethyl)phenyl)-acetonitrile, and tetrabutyl ammonium hydroxide (0.8 M in methanol) were purchased from Alfa Aesar company and used as received. All other agents and solvents were purchased from Aladdin Industrial Corporation and used without further purification. Tetrahydrofuran (THF) was distilled from sodium/benzophenone. Ultrapure water was used in the experiments. Intermediates **1**, **2**, and **3** (Scheme 2) were prepared according to the literature methods.[49,50]

Scheme 2. Synthetic Route of the Cyano-Substituted Diarylethlene Derivatives R-OMe (-H, -CF_3)

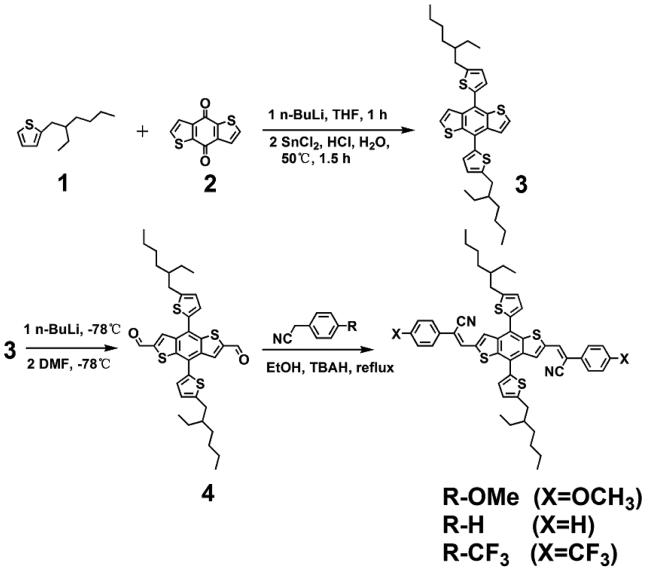

^{1}H NMR and ^{13}C NMR spectra were measured on a JEOL 400 MHz spectrometer [$CDCl_3$ as solvent and tetramethylsilane (TMS) as the internal standard]. Standard MS was obtained on ZAB-HS mass spectrometry or BRUKER micrOTOF-Q II high resolution mass spectrometry. The Fourier transform infrared (FT-IR) spectra were obtained in a transmission mode on a Perkin-Elmer Spectrum 100 spectrometer (Waltham, MA, USA). Typically, 4 scans at a resolution of 1 cm^{-1} were accumulated to obtain one spectrum. UV−visible absorption spectra were recorded on a UV/vis/NIR Perkin-Elmer lambda750 spectrometer (Waltham, MA, USA) using quartz cuvettes of 1 cm path length. Fluorescence spectra were measured on a PE LS-55 spectrometer with a slit width of 3 nm for both excitation and emission. The fluorescence quantum yield values (Φ_F) of the FONs were estimated using quinine sulfate in 0.1 N H_2SO_4 (Φ_F = 54.6%) as standard. Transmission electron microscopy (TEM) images were recorded on a JEM-1200EX microscope operated at 100 kV; the TEM specimens were made by placing a drop of the FONs suspension (100 μg mL^{-1}) on a carbon-coated copper grid. The size distributions measurement of the FONs in phosphate buffer solution (PBS) were determined using a zeta Plus apparatus (ZetaPlus, Brookhaven Instruments, Holtsville, NY).

2.2. Synthesis of 4. **3** (458 mg, 0.79 mmol) was dissolved in anhydrous THF (40 mL) under Ar atmosphere; then, the solution was cooled to −78 °C, and 0.79 mL of n-BuLi (2.5 mol/L in THF) was added, allowing the mixture to react for 1 h with the temperature being raised to room temperature. Then, the mixture was cooled to −78 °C again. Hereafter, 0.3 mL of DMF was added dropwise to the solution for 0.5 h. The solution was stirred at room temperature for 3 h; then, water was added to quench the reaction. The resulting mixture was extracted by dichloromethane. Purification was carried out by column chromatography on silica gel using petroleum ether−dichloromethane (2:1, V/V) as eluent to obtain **4** as orange-red solid (0.35 g, yield 70%). ^{1}H NMR (400 MHz, $CDCl_3$) δ (ppm): 0.89−1.00 (m, 12H, $-CH_3$), 1.29−1.49 (m, 16H, $-CH_2-$), 1.62−1.78 (m, 2H, (methylene)$_3$C−H), 2.89 (d, 4H, J = 6.8 Hz, thienyl-CH_2-), 6.95 (d, 2H, J = 3.6 Hz, thienyl-H), 7.34 (d, 2H, J = 3.6 Hz, thienyl-H), 8.36 (s, 2H, thienyl-H), 10.10 (s, 2H, −CHO); ^{13}C NMR (100 MHz, $CDCl_3$) δ (ppm): 184.8, 147.6, 145.3, 141.4, 138.0, 135.0, 134.2, 128.8, 127.8, 126.0, 41.5, 34.3, 32.6, 29.0, 25.8, 23.1, 14.2, 10.9; IR (cm^{-1}): 2959, 2925, 2859, 1655, 1533, 1486, 1458, 1378, 1326, 1264, 1233, 1137, 1072, 1013, 861, 811; MS (FAB) calcd. for $C_{36}H_{42}O_2S_4$ 634, found 634.

2.3. Synthesis of R-OMe. A solution of **4** (0.12 g, 0.19 mmol) and 2-(4-methoxyphenyl) acetonitrile (0.063 g, 0.43 mmol) in ethanol (10 mL) was stirred at room temperature; then, terabutyl ammonium hydroxide solution (0.8 M, 5 drops) was added to the mixture and heated to reflux temperature for 2 h, resulting a dark red precipitate. The reaction mixture was cooled to room temperature, and the precipitate was filtered and washed with ethanol for several times to obtain a dark red solid **R-OMe** (0.12 g, yield 71%). ^{1}H NMR (400 MHz, $CDCl_3$) δ (ppm): 0.89−1.00 (m, 12H, $-CH_3$), 1.32−1.51 (m, 16H, $-CH_2-$), 1.64−1.77 (m, 2H, (methylene)$_3$C−H), 2.88 (d, 4H, J = 6.8 Hz, thienyl-CH_2-), 3.82 (s, 6H, $-OCH_3$), 6.89−6.97 (m, 6H, thienyl-H, phenyl-H), 7.35 (d, 2H, J = 3.2 Hz, thienyl-H), 7.54 (s, 2H, phenyl-H), 7.56−7.61 (m, 4H, phenyl-H, =CH−), 8.00 (s, 2H, thienyl-H); ^{13}C NMR (100 MHz, $CDCl_3$) δ (ppm): 160.7, 146.7, 139.7, 137.0, 135.9, 132.5, 129.8, 127.4, 126.4, 125.9, 124.7, 117.7, 114.7, 110.8, 55.5, 41.5, 34.4, 32.6, 29.0, 25.8, 23.1, 14.3, 11.0; IR (cm^{-1}): 2958, 2926, 2857, 2212, 1606, 1508, 1462, 1380, 1300, 1256, 1234, 1181, 1160, 1030, 881, 824, 804; HRMS calcd. for $C_{54}H_{56}N_2O_2S_4$, $[M+Na]^+$: 915.3117, found 915.3117.

The syntheses of **R-H** and **R-CF_3** were similar to **R-OMe** and were shown in the Supporting Information.

2.4. Preparation of R-OMe (-H, -CF_3)-F127 FONs. The preparation of **R-OMe (-H, -CF_3)-F127** FONs was carried out as follows.[51] 20 mg of synthesized dyes (**R-OMe (-H, -CF_3)**) was dissolved in 20 mL of THF and then added dropwise under sonication into the solution of Pluronic F127 (50 mg in 20 mL of H_2O in a 100 mL vial) at room temperature. Then, the mixture was evaporated to remove THF completely on a rotary evaporator at 40 °C. The resulting mixture was cooled to room temperature. To remove the excess Pluronic F127, the **R-OMe (-H, -CF_3)-F127** water dispersion was treated by the repeated centrifugal washing process thrice. The concentration of F127 in the analyzed systems is 0.2 mM, which is less than the critical micelle concentration (CMC) of F127 (0.555 mM) at room temperature.[52] The excess F127 can be separated by centrifugation.

2.5. Cytotoxicity of R-OMe (-H, -CF_3)-F127 FONs. The effect of **R-OMe (-H, -CF_3)-F127** FONs to A549 cells was determined via cell morphology observation. In short, cells were seeded in 6-well microplates at a density of 1 × 10^5 cells mL^{-1} in 2 mL of respective media containing 10% FBS. Plates were washed with PBS after cell attachment, and the cells were treated with complete cell culture medium or different concentrations of **R-OMe (-H, -CF_3)-F127** FONs prepared in the media containing 10% FBS for 24 h. Then, all samples were washed with PBS thrice to remove the uninternalized

dx.doi.org/10.1021/am4058309 | ACS Appl. Mater. Interfaces 2014, 6, 3600−3606

FONs. The morphology of cells was observed by an optical microscopy (Leica, Germany), and the overall magnification was 100×.

The cell viability of A549 cells incubated with **R-OMe (-H, -CF_3)-F127** FONs was evaluated by the cell counting kit-8 (CCK-8) assay based on the previous reports.[48] In short, cells were seeded in 96-well microplates at a density of 5 × 10^4 cells mL^{-1} in 160 μL of respective media containing 10% FBS. After cell attachment for 24 h, the cells were incubated with 10, 20, 40, 80, and 120 μg mL^{-1} of **R-OMe (-H, -CF_3)-F127** FONs for 8 and 24 h. Then, the FONs were removed, and cells were washed with PBS thrice. Ten μL of CCK-8 dye and 100 μL of DMEM cell culture medium were added to each well and allowed to incubate for 2 h at 37 °C. Plates were then analyzed by a microplate reader (VictorIII, Perkin-Elmer). Absorption of formazan dye was determined at 450 nm, with the reference wavelength at 620 nm. The values were proportional to the number of live cells. The percent reduction of CCK-8 dye was compared to the controls (cells not stained with **R-OMe (-H, -CF_3)-F127** FONs), which represented 100% CCK-8 reduction. Three replicate wells were applied per microplate, and the experiment was studied thrice. The expression of cell survival was utilizing absorbance relative to that of untreated controls. Results are presented as mean ± standard deviation.

2.6. Confocal Microscopic Imaging of Cells Using R-OMe (-H, -CF_3)-F127 FONs. The confocal microscopic imaging was determined according to the previous reports.[48] In brief, on the day prior to treatment, cells were seeded in a glass bottom dish with a density of 1 × 10^5 cells per dish. On the day of treatment, the cells were incubated with **R-OMe (-H, -CF_3)-F127** FONs at a unified concentration of 100 μg mL^{-1} for 3 h at 37 °C. Afterward, the cells were washed three times with PBS to remove the FONs and then fixed with 4% paraformaldehyde for 10 min at room temperature. Cell images were taken under a Laser Scanning Confocal Microscope (LSCM) Zeiss 710 3-channel (Zeiss, Germany) with the excitation wavelengths of 543 nm.

3. RESULTS AND DISCUSSION

3.1. Charcterization of the Cyano-Substituted Diarylethylene Derivatives. The fluorogens **R-OMe (-H, -CF_3)** were prepared following the synthetic route shown in Scheme 1. Their structures were characterized and confirmed via nuclear magnetic resonance, infrared spectroscopy, and high resolution mass spectrometry. The final step yields ranged from 71% to 82%. The obtained fluorescent dyes **R-OMe (-H, -CF_3)** were hydrophobic and emitted strong crimson fluorescence in solid state, while their fluorescent wavelength in THF decreased, which showed yellow or orange (Figures 1A, S1A, and S2A, Supporting Information). The AIEE characteristic of **R-OMe** was shown in Figure S3, Supporting Information, which indicated an obvious AIEE effect. The same AIEE effect was observed for **R-CF_3** (Figure S5, Supporting Information). However, **R-H** did not show AIEE effect (Figure S4, Supporting Information). Meanwhile, the PL spectra of **R-OMe (-H, CF_3)** in THF with different concentrations were determined and shown in Figures S6−8, Supporting Information, which demonstrated that the concentration effect could not give rise to AIEE effect. After hydrophobic interaction with surfactant Pluronic F127, the dyes could be dispersed well in water and the fluorogens aggregate into cores to form FONs. Such **R-OMe-F127** FONs emitted strong red fluorescence in water with a 14% proportionate increase of fluorescent intensity than **R-OMe** in a pure THF solution (Figure 1A). The fluorescence quantum yield of the **R-OMe-F127** FONs was as high as 20% using quinine sulfate as a reference dye. **R-H-F127** and **R-CF_3-F127** FONs also emitted strong red fluorescence in water with almost the same fluorescent intensity as **R-H** and **R-CF_3** in THF (Figures S1A and S2A, Supporting Information), and their quantum yields were determined as 12% and 25% respectively, confirming the obvious anti-ACQ features.

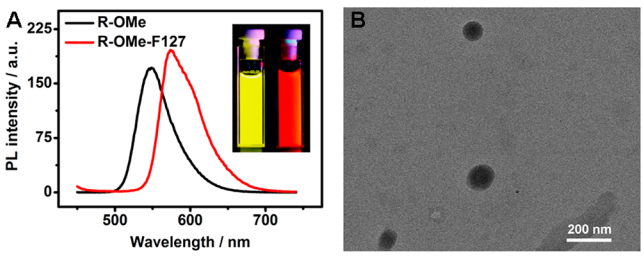

Figure 1. (A) Fluorescence spectra of **R-OMe** in THF and **R-OMe-F127** dispersed in water at room temperature; concentration = 10^{-5} M. Inset: fluorescent image of **R-OMe** in THF and **R-OMe-F127** in water taken at 365 nm UV light. (B) TEM image of **R-OMe-F127** FONs (100 μg mL^{-1}) dispersed in water; scale bar = 200 nm.

As shown in the inset of Figure 1A, after hydrophobic−hydrophilic interaction with Pluronic F127, the surfactant modified **R-OMe-F127** FONs were readily dispersed in water, suggesting the successful formation of hydrophilic red FONs with excellent water dispersibility. FT-IR spectra showed that a peak centered at 1110 cm^{-1}, which is corresponding to the stretch vibration of C−O bond, was significantly enhanced in **R-OMe-F127** FONs, demonstrating the successful formation of the complex combining Pluronic F127 with **R-OMe** dyes (Figure S9, Supporting Information). The C−O stretch vibration was also observed significantly enhanced in the FT-IR spectra of **R-H-F127** and **R-CF_3-F127** (Figures S10 and S11, Supporting Information), also confirming the successful encapsulation. The TEM images further confirmed the formation of the FONs. Some small organic spheres with diameters ranging from 60 to 100 nm were observed, which represented the assembly of **R-OMe (-H, -CF_3)** and Pluronic F127 (Figures 1B, S1B, and S2B, Supporting Information). The dynamic light scattering (DLS) experiment has been carried out to determine the size distribution of **R-OMe-F127** FONs in PBS. The results showed the size distribution was 166.0 ± 8.8 nm, with a polydispersity index (PDI) of 0.226. Meanwhile, the size distributions of **R-H-F127** and **R-CF_3-F127** FONs were also determined as 198.7 ± 10.9 and 187.3 ± 4.1 nm, with PDIs of 0.184 and 0.201, respectively. The sizes characterized by TEM were somewhat smaller than those measured by the zeta Plus particle size analyzer, which was likely due to the shrinkage of micelle during the drying process. The formation of such nanoaggregates was probably due to the strong interaction between the hydrophobic segments of F127 and the alkyl chain of **R-OMe (-H, -CF_3)**; further, the hydrophilic segments of Pluronic F127 covered the surface to create a water-soluble periphery.

When the nanoparticles formed, the fluorescent emission wavelength of the FONs emerged a 26, 41, and 23 nm red-shift for **R-OMe-F127**, **R-H-F127**, and **R-CF_3-F127**, respectively, compared with **R-OMe (-H, -CF_3)** in THF. The red-shift phenomenon also could be observed in the THF−water mixtures at high water fraction, which might represent the formation of aggregates (Figures S3−5, Supporting Information). The above observed spectra shifts are presumably attributed to the torsion-locking planarization of the distorted solution geometry of the synthesized compounds by aggregation, which narrows the optical bandgap by increasing the effective π-electron conjugation. The appearance of a

longer-wavelength emission also suggests that close stacking of the planarized molecules is possibly accompanied with enhanced fluorescence of J-type π-aggregation, which often occurrs in cyano-substituted diarylethlene derivatives.[53] To better understand the different red-shift values for the above three compounds, we performed quantum mechanical computations with a Gaussian 03 software.[54] On the basis of the density functional method at the B3LYP/6-31G level after optimizing the structure, the lowest energy spatial conformation of these compounds were obtained. As shown in Figure 2,

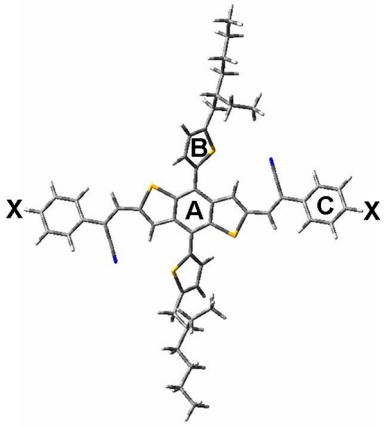

Figure 2. Schematic diagram for the optimization geometries of the compounds (X represents the **-OMe**, **-H**, or **-CF_3** group).

all the compounds show twist configurations. Dihedral angles between two aryl rings (A, B, or C) as defined in Figure 2 were calculated, A−B for these three compounds were all 55°. However, the dihedral angles for A−C exhibit divergences, which were 28°, 36°, and 28° for **R-OMe**, **R-H**, and **R-CF_3**, respectively. These results are well consistent with the different red-shift values of these compounds and thus also verify the above assumption of planarization. It was also suggested by some previous references that the differences of the peripheral substituted groups in the compounds caused the different twisted spatial conformation due to the steric effect and ultimately resulted in the different shifts of the emission wavelength.[55,56]

UV absorption and PL excitation spectra were recorded to investigate the optical properties of these compounds and their resulting FONs. Figure 3A shows that the UV absorption of compound **R-OMe** had multiple peaks, which represented the different conjugated chromophore groups. The highest absorption wavelength was located at 486 nm, indicating a completely conjugated system. Meanwhile, the UV absorption

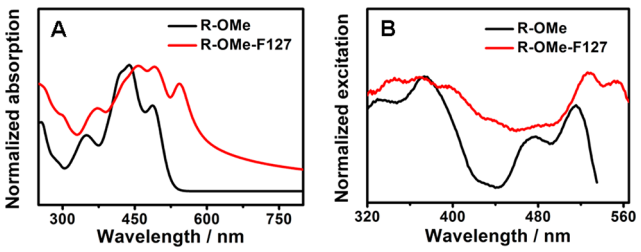

Figure 3. (A) Normalized UV absorption and (B) normalized PL excitation of **R-OMe** (in THF, 100 μg mL^{-1}) and **R-OMe-F127** (in water, 100 μg mL^{-1}) at room temperature.

of **R-OMe-F127** FONs also had similar multiple peaks, although overall red-shifts simultaneously appeared. The highest absorption moved to 542 nm with a red-shift of 56 nm. A similar phenomenon appeared in the **R-H-F127** and **R-CF_3-F127** FONs with a red-shift of 72 and 62 nm, respectively (Figures S12A and S13A, Supporting Information). The red-shift difference of these three composites may be due to the different twisted spatial conformations of the compounds. UV spectra of **R-OMe** (**-H**, **-CF_3**)**-F127** FONs in water with different concentrations were determined, indicating that the highest absorption wavelength did not change at different concentrations (Figures S14−16, Supporting Information). In other words, the highest absorption wavelengths of the FONs were not significantly affected by the scattering effect.

As shown in Figure 3B, multiple peaks were also observed in the PL excitation spectrum of **R-OMe** with a valley at 440 nm. When the wavelength reached 515 nm, the excitation began to decline. However, the excitation spectrum of **R-OMe-F127** in water was very different compared to that of **R-OMe** in THF. The excitation intensity of **R-OMe-F127** continued to rise even when the wavelength exceeded 515 nm and maintained high excitation intensity until 565 nm, indicating broad excitation wavelength. This long-wave excitation feature is greatly beneficial for its cell imaging application, which can reduce the damage to the organism. **R-H-F127** and **R-CF_3-F127** FONs also exhibited similar broad excitation wavelength, providing them superiority for application in the bioimaging field (Figures S12B and S13B, Supporting Information).

The absorption and PL excitation spectra in Figure 3 also showed a lot of scattering, suggesting that larger aggregates were formed. This was also confirmed by the TEM and zeta Plus particle size analyzer results. In other words, the small spheres particle was believed to be part of the aggregates. When we compared the UV absorption spectra with PL emission spectra of these synthesized compounds, we noticed that their highest absorption wavelength were very close to each other, which were 486, 484, and 488 nm for **R-OMe**, **R-H**, and **R-CF_3**, respectively. However, their PL emission wavelengths exhibit large Stokes shift. In order to understand the reason of the differences between UV absorption and PL emission spectra, we utilized a Gaussian 03 software to perform quantum mechanical computations of the compounds. The highest occupied molecular orbitals (HOMOs) and the lowest unoccupied molecular orbitals (LUMOs) of these compounds were calculated according to the density functional method at the B3LYP/6-31G level after structural optimization (Figure 4).[54]

The HOMOs of **R-OMe** showed dispersed electron cloud distributions on the entire thiophene and benzene conjugated groups, whereas the electron cloud of the LUMOs showed reduced distribution on the thiophene groups and increased distribution on the cyano groups. The HOMOs of **R-H** exhibited dispersed electron cloud distributions on the whole thiophene groups and partial benzene groups, whereas the electron cloud of the LUMOs showed decreased distribution on the thiophene groups and increased distribution on the cyano and benzene groups, indicating more electron cloud flow from HOMOs to LUMOs than that of **R-OMe**. However, the HOMOs of **R-CF_3** observed no electron cloud distribution on the peripheral phenyl groups. As shown in the LUMOs, the electron cloud flowed from the direction of thiophene groups to the peripheral phenyl and cyano groups, confirming that most electron clouds flow from HOMOs to LUMOs. This

dx.doi.org/10.1021/am4058309 | ACS Appl. Mater. Interfaces 2014, 6, 3600−3606

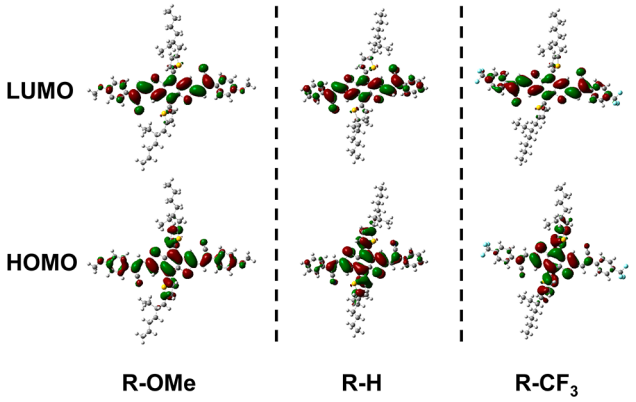

Figure 4. Calculated spatial electron distributions of LUMOs and HOMOs of the compounds.

result might provide an explanation of the different Stokes shift of three compounds.

3.2. Biocompatibility. To test the potential of **R-OMe (-H, -CF_3)-F127** FONs for biomedical applications, their biocompatibilities with A549 cells were subsequently investigated. Figure 5A–C represented the microscopy images of

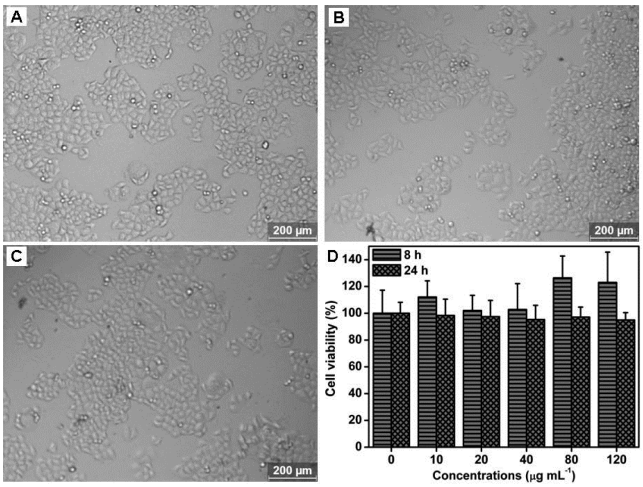

Figure 5. Biocompatibility evaluations of **R-OMe-F127** FONs. (A–C) optical microscopy images of A549 cells incubated with different concentrations of **R-OMe-F127** FONs for 24 h: (A) control cells, (B) 40 μg mL^{-1}, (C) 120 μg mL^{-1}; (D) cell viability of **R-OMe-F127** FONs with A549 cells for 8 and 24 h, respectively. Cell viability was determined by the WST assay.

cells when incubated with different concentrations of **R-OMe-F127** FONs for 24 h. No significant cell morphology changes were observed. It seemed that cells still attached very well to the cell plate even at high concentrations of **R-OMe-F127** FONs, which were up to 120 μg mL^{-1}. The optical microscopy images implied good biocompatibility of **R-OMe-F127** FONs. Cell viability of **R-OMe-F127** FONs was further carried out to quantitatively evaluate the biocompatibility of **R-OMe-F127** FONs (Figure 5D). The results showed that no obvious cell viability decrease was found when cells were incubated with 80 μg mL^{-1} of **R-OMe-F127** FONs for 24 h, the cell viability even unexpectedly reached up to 120% for 8 h. The cell viability value for 24 h was about 95% and even the concentration increased to 120 μg mL^{-1}, which further confirmed the excellent biocompatibility of **R-OMe-F127** FONs. The biocompatibility evaluations of **R-H-F127** and **R-CF_3-F127** FONs were shown in Figures S17 and S18, Supporting Information, which also demonstrated excellent biocompatibility, as the cell viability values for 24 h were >90% even when the concentrations increased to 120 μg mL^{-1}. In the recent report, targeted nanoparticles encapsulated with different drugs and functionalized with various ligands that had high affinity and specificity had been shown to efficiently accumulate in specific tissues and dramatically increased the therapeutic efficacy of long-circulating nanoparticle drug delivery systems.[51,57] Furthermore, many other components including therapeutic drugs and targeting agents, which contain a reactive group like acyl chloride, acid anhydride, or carboxyl group, could be further incorporated into these bright red FONs due to the existing reactive hydroxyl groups derived from the end-groups of F127. In addition to the biocompatibility of F127 funtionalized FONs, in vivo circulation, clearance, and biodistribution of these FONs could be envisaged to construct a multifunctional platform for drug vectorization applications.

3.3. Cell Imaging. The cell imaging applications of **R-OMe-F127** FONs were further investigated. The LSCM images of cells incubated with 100 μg mL^{-1} of **R-OMe-F127** FONs for 3 h were shown in Figure 6. Bright field images indicated that

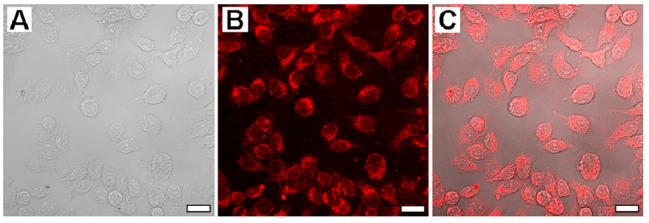

Figure 6. LSCM images of A549 cells incubated with 100 μg mL^{-1} of **R-OMe-F127** FONs for 3 h. (A) Bright field image, (B) fluorescent image which was excited with a 543 nm laser, and (C) merged images. Scale bar = 20 μm.

cells still maintained their normal morphology, which further confirmed the good biocompatibility of **R-OMe-F127** FONs. When cells were excited with the 543 nm laser, the cell uptake of **R-OMe-F127** FONs can be clearly distinguished from the cell environment due to the successful staining of the **R-OMe-F127** FONs. Furthermore, many dark areas could also be found in the cells from LSCM images, which were likely to be the locations of the cell nucleus. The LSCM images of A549 cells incubated with **R-H-F127** and **R-CF_3-F127** FONs also demonstrated the good biocompatibilities (Figures S19 and S20, Supporting Information). In a previous report,[58] amphiphilic block copolymers were employed to disperse hydrophobic AIE dyes to form polymeric micelles; thus, FONs were then used for intracellular imaging. Phagocytosis was regarded as the possible mechanism for intracellular uptake by the cell, while the micelles could remain intact in the cells. In our work, phagocytosis might also be the possible mechanism for intracellular uptake by A549 cells. Since the size of FONs was bigger than that of the nucleus pore (9 × 15 nm), these considered FONs could not directly enter the cell nucleus. Therefore, we could expect that the prepared red FONs should be promising candidates for various biomedical applications due to the combined superiorities for bioapplications, such as unique PL properties, good water solubility, excellent biocompatibility, and biodegradable potential.

4. CONCLUSIONS

In summary, three cyano-substituted diarylethlene derivatives **R-OMe** (**-H**, **-CF_3**) with different peripherally substituted groups were synthesized in high yield and facilely prepared as red FONs via hydrophobic−hydrophilic interactions with Pluronic F127. Such red FONs exhibited anti-ACQ property and broad excitation wavelength, and their PL properties could be modulated by distinct substituted groups. Red FONs with diameter from 60 to 100 nm could be easily obtained. Their biocompatibilities and cell imaging applications were further investigated. Our results demonstrate that such red FONs possess excellent water solubilities and biocompatibilities, which are promising for bioimaging applications.

■ ASSOCIATED CONTENT

Ⓢ Supporting Information

Synthesis of **R-H** and **R-CF_3**, fluorescence spectra, TEM images, FT-IR spectra, UV absorption, PL excitation spectra, biocompatibility evaluations, and CLSM images of **R-H-F127** and **R-CF_3-F127**. The AIEE characteristic of **R-OMe** (**-H**, **-CF_3**), PL spectra of **R-OMe** (**-H**, **-CF_3**) in THF with different concentrations, and UV spectra of **R-OMe** (**-H**, **-CF_3**)**-F127** dispersed in water with different concentrations. This material is available free of charge via the Internet at http://pubs.acs.org.

■ AUTHOR INFORMATION

Corresponding Authors

*E-mail: sychyzhang@126.com.

*E-mail: weiyen@tsinghua.edu.cn.

Author Contributions

[#]Xiqi Zhang and Xiaoyong Zhang contributed equally to this work.

Notes

The authors declare no competing financial interest.

■ ACKNOWLEDGMENTS

This research was supported by the National Science Foundation of China (Nos. 21134004, 21201108, 51363016), the National 973 Project (No. 2011CB935700), and China Postdoctoral Science Foundation (Nos. 2013T60100, 2012M520243).

■ REFERENCES

(1) Weissleder, R.; Pittet, M. J. Imaging in the Era of Molecular Oncology. *Nature* **2008**, *452*, 580−589.

(2) Wang, F.; Banerjee, D.; Liu, Y.; Chen, X.; Liu, X. Upconversion Nanoparticles in Biological Labeling, Imaging, and Therapy. *Analyst* **2010**, *135*, 1839−1854.

(3) Lee, S.; Cha, E. J.; Park, K.; Lee, S. Y.; Hong, J. K.; Sun, I. C.; Kim, S. Y.; Choi, K.; Kwon, I. C.; Kim, K. A Near-Infrared-Fluorescence-Quenched Gold-Nanoparticle Imaging Probe for *in vivo* Drug Screening and Protease Activity Determination. *Angew. Chem., Int. Ed.* **2008**, *120*, 2846−2849.

(4) Chandra, S.; Das, P.; Bag, S.; Laha, D.; Pramanik, P. Synthesis, Functionalization and Bioimaging Applications of Highly Fluorescent Carbon Nanoparticles. *Nanoscale* **2011**, *3*, 1533−1540.

(5) Díez, I.; Ras, R. H. Fluorescent Silver Nanoclusters. *Nanoscale* **2011**, *3*, 1963−1970.

(6) Shu, X.; Royant, A.; Lin, M. Z.; Aguilera, T. A.; Lev-Ram, V.; Steinbach, P. A.; Tsien, R. Y. Mammalian Expression of Infrared Fluorescent Proteins Engineered from a Bacterial Phytochrome. *Science* **2009**, *324*, 804−807.

(7) Lin, H. H.; Chan, Y. C.; Chen, J. W.; Chang, C. C. Aggregation-Induced Emission Enhancement Characteristics of Naphthalimide Derivatives and Their Applications in Cell Imaging. *J. Mater. Chem.* **2011**, *21*, 3170−3177.

(8) Cai, Z.; Ye, Z.; Yang, X.; Chang, Y.; Wang, H.; Liu, Y.; Cao, A. Encapsulated Enhanced Green Fluorescence Protein in Silica Nanoparticle for Cellular Imaging. *Nanoscale* **2011**, *3*, 1974−1976.

(9) Resch-Genger, U.; Grabolle, M.; Cavaliere-Jaricot, S.; Nitschke, R.; Nann, T. Quantum Dots versus Organic Dyes as Fluorescent Labels. *Nat. Methods* **2008**, *5*, 763−775.

(10) Kairdolf, B. A.; Smith, A. M.; Stokes, T. D.; Wang, M. D.; Young, A. N.; Nie, S. Semiconductor Quantum Dots for Bioimaging and Biodiagnostic Applications. *Annu. Rev. Anal. Chem.* **2013**, *6*, 143−162.

(11) Lin, H. H.; Su, S. Y.; Chang, C. C. Fluorescent Organic Nanoparticle Formation in Lysosomes for Cancer Cell Recognition. *Org. Biomol. Chem.* **2009**, *7*, 2036−2039.

(12) Yu, Y.; Feng, C.; Hong, Y.; Liu, J.; Chen, S.; Ng, K. M.; Luo, K. Q.; Tang, B. Z. Cytophilic Fluorescent Bioprobes for Long-Term Cell Tracking. *Adv. Mater.* **2011**, *23*, 3298−3302.

(13) Yu, Y.; Hong, Y.; Feng, C.; Liu, J.; Lam, J.; Faisal, M.; Ng, K.; Luo, K.; Tang, B. Synthesis of an AIE-Active Fluorogen and Its Application in Cell Imaging. *Sci. China B* **2009**, *52*, 15−19.

(14) Feng, L.; Zhu, C.; Yuan, H.; Liu, L.; Lv, F.; Wang, S. Conjugated Polymer Nanoparticles: Preparation, Properties, Functionalization and Biological Applications. *Chem. Soc. Rev.* **2013**, *42*, 6620−6633.

(15) Zhu, C.; Yang, Q.; Lv, F.; Liu, L.; Wang, S. Conjugated Polymer-Coated Bacteria for Multimodal Intracellular and Extracellular Anticancer Activity. *Adv. Mater.* **2013**, *25*, 1203−1208.

(16) Nie, C.; Zhu, C.; Feng, L.; Lv, F.; Liu, L.; Wang, S. Synthesis of a New Conjugated Polymer for DNA Alkylation and Gene Regulation. *ACS Appl. Mater. Interfaces* **2013**, *5*, 4549−4554.

(17) Wang, B.; Zhu, C.; Liu, L.; Lv, F.; Yang, Q.; Wang, S. Synthesis of a New Conjugated Polymer for Cell Membrane Imaging by Using an Intracellular Targeting Strategy. *Polym. Chem.* **2013**, *4*, 5212−5215.

(18) Lu, X.; Jiang, R.; Yang, M.; Fan, Q.; Hu, W.; Zhang, L.; Yang, Z.; Deng, W.; Shen, Q.; Huang, Y.; Liu, X.; Huang, W. Monodispersed Grafted Conjugated Polyelectrolyte-Stabilized Magnetic Nanoparticles as Multifunctional Platform for Cellular Imaging and Drug Delivery. *J. Mater. Chem. B* **2014**, *2*, 376−386.

(19) Zhang, G.; Lu, X.; Wang, Y.; Huang, Y.; Fan, Q.; Huang, W. Water-Soluble Fluorescent Nanoparticles without Distinct Aggregation of Conjugated Polymer Chains. *Polym. Int.* **2010**, *60*, 45−50.

(20) Zhang, P.; Chen, J.; Huang, F.; Zeng, Z.; Hu, J.; Yi, P.; Zeng, F.; Wu, S. One-pot Fabrication of Polymer Nanoparticle-Based Chemosensors for Cu^{2+} Detection in Aqueous Media. *Polym. Chem.* **2013**, *4*, 2325−2332.

(21) Sugihara, S.; Armes, S. P.; Blanazs, A.; Lewis, A. L. Non-Spherical Morphologies from Cross-Linked Biomimetic Diblock Copolymers using RAFT Aqueous Dispersion Polymerization. *Soft Matter* **2011**, *7*, 10787−10793.

(22) Yin, M.; Feng, C.; Shen, J.; Yu, Y.; Xu, Z.; Yang, W.; Knoll, W.; Müllen, K. Dual-Responsive Interaction to Detect DNA on Template-Based Fluorescent Nanotubes. *Small* **2011**, *7*, 1629−1634.

(23) Cui, K.; Lu, X.; Cui, W.; Wu, J.; Chen, X.; Lu, Q. Fluorescent Nanoparticles Assembled from a Poly(Ionic Liquid) for Selective Sensing of Copper Ions. *Chem. Commun.* **2011**, *47*, 920−922.

(24) Luo, J.; Lei, T.; Wang, L.; Ma, Y.; Cao, Y.; Wang, J.; Pei, J. Highly Fluorescent Rigid Supramolecular Polymeric Nanowires Constructed Through Multiple Hydrogen Bonds. *J. Am. Chem. Soc.* **2009**, *131*, 2076−2077.

(25) Shi, C.; Guo, Z.; Yan, Y.; Zhu, S.; Xie, Y.; Zhao, Y. S.; Zhu, W.; Tian, H. Self-Assembly Solid-State Enhanced Red Emission of Quinolinemalononitrile: Optical Waveguides and Stimuli Response. *ACS Appl. Mater. Interfaces* **2013**, *5*, 192−198.

(26) Liu, J.; Ding, D.; Geng, J.; Liu, B. PEGylated Conjugated Polyelectrolytes Containing 2,1,3-Benzoxadiazole Units for Targeted Cell Imaging. *Polym.Chem.* **2012**, *3*, 1567−1575.

(27) Zhang, X.; Zhang, X.; Wang, S.; Liu, M.; Zhang, Y.; Tao, L.; Wei, Y. Facile Incorporation of Aggregation-Induced Emission Materials into Mesoporous Silica Nanoparticles for Intracellular

Imaging and Cancer Therapy. *ACS Appl. Mater. Interfaces* **2013**, *5*, 1943−1947.
(28) Mahtab, F.; Yu, Y.; Lam, J. W.; Liu, J.; Zhang, B.; Lu, P.; Zhang, X.; Tang, B. Z. Fabrication of Silica Nanoparticles with Both Efficient Fluorescence and Strong Magnetization and Exploration of Their Biological Applications. *Adv. Funct. Mater.* **2011**, *21*, 1733−1740.
(29) Shi, H.; Kwok, R. T.; Liu, J.; Xing, B.; Tang, B. Z.; Liu, B. Real-Time Monitoring of Cell Apoptosis and Drug Screening Using Fluorescent Light-Up Probe with Aggregation-Induced Emission Characteristics. *J. Am. Chem. Soc.* **2012**, *134*, 17972−17981.
(30) Zhang, X.; Liu, M.; Yang, B.; Zhang, X.; Wei, Y. Tetraphenylethene-Based Aggregation-Induced Emission Fluorescent Organic Nanoparticles: Facile Preparation and Cell Imaging Application. *Colloids Surf., B: Biointerfaces* **2013**, *112*, 81−86.
(31) Leung, C. W. T.; Hong, Y.; Chen, S.; Zhao, E.; Lam, J. W. Y.; Tang, B. Z. A Photostable AIE Luminogen for Specific Mitochondrial Imaging and Tracking. *J. Am. Chem. Soc.* **2013**, *135*, 62−65.
(32) Zhang, X.; Liu, M.; Yang, B.; Zhang, X.; Chi, Z.; Liu, S.; Xu, J.; Wei, Y. Cross-Linkable Aggregation Induced Emission Dye Based Red Fluorescent Organic Nanoparticles and Their Cell Imaging Applications. *Polym. Chem.* **2013**, *4*, 5060−5064.
(33) Wang, Z.; Chen, S.; Lam, J. W. Y.; Qin, W.; Kwok, R. T. K.; Xie, N.; Hu, Q.; Tang, B. Z. Long-Term Fluorescent Cellular Tracing by the Aggregates of AIE Bioconjugates. *J. Am. Chem. Soc.* **2013**, *135*, 8238−8245.
(34) Zhang, X.; Zhang, X.; Yang, B.; Hui, J.; Liu, M.; Chi, Z.; Liu, S.; Xu, J.; Wei, Y. Facile Preparation and Cell Imaging Applications of Fluorescent Organic Nanoparticles That Combine AIE Dye and Ring-Opening Polymerization. *Polym. Chem.* **2014**, *5*, 318−322.
(35) Luo, J.; Xie, Z.; Lam, J. W. Y.; Cheng, L.; Chen, H.; Qiu, C.; Kwok, H. S.; Zhan, X.; Liu, Y.; Zhu, D.; Tang, B. Z. Aggregation-Induced Emission of 1-Methyl-1,2,3,4,5-Pentaphenylsilole. *Chem. Commun.* **2001**, *37*, 1740−1741.
(36) An, B. K.; Kwon, S. K.; Jung, S. D.; Park, S. Y. Enhanced Emission and Its Switching in Fluorescent Organic Nanoparticles. *J. Am. Chem. Soc.* **2002**, *124*, 14410−14415.
(37) Zhang, X.; Ma, Z.; Liu, M.; Zhang, X.; Jia, X.; Wei, Y. A New Organic Far-Red Mechanofluorochromic Compound Derived from Cyano-Substituted Diarylethene. *Tetrahedron* **2013**, *69*, 10552−10557.
(38) Xue, W.; Zhang, G.; Zhang, D.; Zhu, D. A New Label-Free Continuous Fluorometric Assay for Trypsin and Inhibitor Screening with Tetraphenylethene Compounds. *Org. Lett.* **2010**, *12*, 2274−2277.
(39) Zhang, X.; Chi, Z.; Li, H.; Xu, B.; Li, X.; Liu, S.; Zhang, Y.; Xu, J. Synthesis and Properties of Novel Aggregation-Induced Emission Compounds with Combined Tetraphenylethylene and Dicarbazolyl Triphenylethylene Moieties. *J. Mater. Chem.* **2011**, *21*, 1788−1796.
(40) Zhang, X.; Chi, Z.; Li, H.; Xu, B.; Li, X.; Zhou, W.; Liu, S.; Zhang, Y.; Xu, J. Piezofluorochromism of An Aggregation-Induced Emission Compound Derived from Tetraphenylethylene. *Chem.-Asian J.* **2011**, *6*, 808−811.
(41) Zhang, X.; Chi, Z.; Zhang, Y.; Liu, S.; Xu, J. Recent Advances in Mechanochromic Luminescent Metal Complexes. *J. Mater. Chem. C* **2013**, *1*, 3376−3390.
(42) Zhang, X.; Yang, Z.; Chi, Z.; Chen, M.; Xu, B.; Wang, C.; Liu, S.; Zhang, Y.; Xu, J. A Multi-Sensing Fluorescent Compound Derived from Cyanoacrylic Acid. *J. Mater. Chem.* **2009**, *20*, 292−298.
(43) Zhang, X.; Chi, Z.; Xu, B.; Li, H.; Yang, Z.; Li, X.; Liu, S.; Zhang, Y.; Xu, J. Synthesis of Blue Light Emitting Bis (triphenylethylene) Derivatives: A Case of Aggregation-Induced Emission Enhancement. *Dyes Pigm.* **2011**, *89*, 56−62.
(44) He, J.; Xu, B.; Chen, F.; Xia, H.; Li, K.; Ye, L.; Tian, W. Aggregation-Induced Emission in the Crystals of 9,10-Distyrylanthracene Derivatives: The Essential Role of Restricted Intramolecular Torsion. *J. Phys. Chem. C* **2009**, *113*, 9892−9899.
(45) Zhang, X.; Chi, Z.; Xu, B.; Chen, C.; Zhou, X.; Zhang, Y.; Liu, S.; Xu, J. End-Group Effects of Piezofluorochromic Aggregation-Induced Enhanced Emission Compounds Containing Distyrylanthracene. *J. Mater. Chem.* **2012**, *22*, 18505−18513.
(46) Zhang, X.; Chi, Z.; Xu, B.; Jiang, L.; Zhou, X.; Zhang, Y.; Liu, S.; Xu, J. Multifunctional Organic Fluorescent Materials Derived from 9,10-Distyrylanthracene with Alkoxyl Endgroups of Various Lengths. *Chem. Commun.* **2012**, *48*, 10895−10897.
(47) Zhang, X.; Ma, Z.; Yang, Y.; Zhang, X.; Chi, Z.; Liu, S.; Xu, J.; Jia, X.; Wei, Y. Influence of Alkyl Length on Properties of Piezofluorochromic Aggregation Induced Emission Compounds Derived from 9,10-Bis[(N-alkylphenothiazin-3-yl)vinyl]anthracene. *Tetrahedron* **2014**, *70*, 924−929.
(48) Zhang, X.; Zhang, X.; Wang, S.; Liu, M.; Tao, L.; Wei, Y. Surfactant Modification of Aggregation-Induced Emission Material as Biocompatible Nanoparticles: Facile Preparation and Cell Imaging. *Nanoscale* **2013**, *5*, 147−150.
(49) Ellinger, S.; Ziener, U.; Thewalt, U.; Landfester, K.; Möller, M. Synthesis and Self-Organization of α, ω-Substituted Oligothiophenes with Long, Branched Alkyl Substituents. *Chem. Mater.* **2007**, *19*, 1070−1075.
(50) Huo, L.; Zhang, S.; Guo, X.; Xu, F.; Li, Y.; Hou, J. Replacing Alkoxy Groups with Alkylthienyl Groups: A Feasible Approach to Improve the Properties of Photovoltaic Polymers. *Angew. Chem., Int. Ed.* **2011**, *123*, 9871−9876.
(51) Basak, R.; Bandyopadhyay, R. Encapsulation of Hydrophobic Drugs in Pluronic F127 Micelles: Effects of Drug Hydrophobicity, Solution Temperature, and pH. *Langmuir* **2013**, *29*, 4350−4356.
(52) Alexandridis, P.; Holzwarth, J. F.; Hatton, T. A. Micellization of Poly (Ethylene Oxide)-Poly (Propylene Oxide)-Poly (Ethylene Oxide) Triblock Copolymers in Aqueous Solutions: Thermodynamics of Copolymer Association. *Macromolecules* **1994**, *27*, 2414−2425.
(53) An, B. K.; Gihm, S. H.; Chung, J. W.; Park, C. R.; Kwon, S. K.; Park, S. Y. Color-Tuned Highly Fluorescent Organic Nanowires/Nanofabrics: Easy Massive Fabrication and Molecular Structural Origin. *J. Am. Chem. Soc.* **2009**, *131*, 3950−3957.
(54) Frisch, M. J.; Trucks, G. W.; Schlegel, H. B. *Gaussian 03, revision D.01*; Gaussian, Inc.: Wallingford, CT, 2004.
(55) Zhang, X.; Chi, Z.; Zhang, J.; Li, H.; Xu, B.; Li, X.; Liu, S.; Zhang, Y.; Xu, J. Piezofluorochromic Properties and Mechanism of an Aggregation-Induced Emission Enhancement Compound Containing N-Hexyl-Phenothiazine and Anthracene Moieties. *J. Phys. Chem. B* **2011**, *115*, 7606−7611.
(56) Zhang, X.; Chi, Z.; Zhou, X.; Liu, S.; Zhang, Y.; Xu, J. Influence of Carbazolyl Groups on Properties of Piezofluorochromic Aggregation-Enhanced Emission Compounds Containing Distyrylanthracene. *J. Phys. Chem. C* **2012**, *116*, 23629−23638.
(57) Alexis, F.; Pridgen, E.; Molnar, L. K.; Farokhzad, O. C. Factors Affecting the Clearance and Biodistribution of Polymeric Nanoparticles. *Mol. Pharmaceutics* **2008**, *5*, 505−515.
(58) Wu, W.-C.; Chen, C.-Y.; Tian, Y.; Jang, S.-H.; Hong, Y.; Liu, Y.; Hu, R.; Tang, B. Z.; Lee, Y.-T.; Chen, C.-T.; Chen, W.-C.; Jen, A. K. Y. Enhancement of Aggregation-Induced Emission in Dye-Encapsulating Polymeric Micelles for Bioimaging. *Adv. Funct. Mater.* **2010**, *20*, 1413−1423.